optica

Scattering-free channels of invisibility across non-Hermitian media: supplementary material

K. G. MAKRIS[1,2*], I. KREŠIĆ[3], A. BRANDSTÖTTER[3], AND S. ROTTER[3]

[1] ITCP-Physics Department, University of Crete, Heraklion, 71003, Greece
[2] Institute of Electronic Structure and Lasers (IESL), Foundation for Research and Technology - Hellas, 71110 Heraklion, Greece
[3] Institute for Theoretical Physics, Vienna University of Technology, A-1040, Vienna, Austria
[*] Corresponding author: makris@physics.uoc.gr

Compiled June 3, 2020

This document provides supplementary information to "Scattering-free channels of invisibility across non-Hermitian media," https://doi.org/10.1364/OPTICA.390788. In particular, we provide detailed analytical derivations that are crucial for the completeness and understanding of the main results of the paper, together with additional numerical simulations to verify our approach.

1. NON-HERMITIAN MAPPING OF TWO-DIMENSIONAL WAVES

A. Derivation of the dielectric function

Here we derive Eq. (4) of the main paper. We start our analysis with the two dimensional scalar Helmholtz equation that describes scattering of waves in an inhomogeneous landscape,

$$\frac{\partial^2 E}{\partial x^2} + \frac{\partial^2 E}{\partial y^2} + k^2[n_{ref}^2 + \varepsilon(x,y)]E = 0\,. \tag{S1}$$

The corresponding Helmholtz wave equation in a homogeneous (bulk) space is the following:

$$\frac{\partial^2 \phi}{\partial x^2} + \frac{\partial^2 \phi}{\partial y^2} + k^2 n_{ref}^2 \phi = 0\,, \tag{S2}$$

where n_{ref}^2 is the background dielectric permittivity without any spatial dependence. We are interested in connecting these two solutions through the transformation:

$$E(x,y) = \phi(x,y)e^{ik\theta(x,y)}. \tag{S3}$$

The transformation ensures that the two solutions of two different wave equations have exactly the same intensity profiles, $|E(x,y)|^2 = |\phi(x,y)|^2$.

For the first derivatives we find,

$$E_x = (\phi_x + ik\phi\theta_x)\, e^{ik\theta} \tag{S4}$$

$$E_y = \left(\phi_y + ik\phi\theta_y\right) e^{ik\theta}\,, \tag{S5}$$

while for the second derivatives we obtain,

$$E_{xx} = (\phi_{xx} + ik\theta_{xx}\phi + 2ik\theta_x\phi_x - k^2\theta_x^2\phi)e^{ik\theta} \tag{S6}$$

$$E_{yy} = (\phi_{yy} + ik\theta_{yy}\phi + 2ik\theta_y\phi_y - k^2\theta_y^2\phi)e^{ik\theta}\,, \tag{S7}$$

where the subscripts "x, y" and "xx, yy" denote the first and second derivatives in the corresponding coordinates, respectively. By substitution into Eq. (S1) we finally get for $\varepsilon(x,y)$:

$$\varepsilon(x,y) = (\nabla\theta)^2 - \frac{i}{k}\left(\nabla^2\theta + 2\nabla\theta \cdot \frac{\nabla\phi}{\phi}\right). \tag{S8}$$

At this point we have to note that the last term of the above equation contributes to both the real and imaginary parts of $\varepsilon(x,y)$, since ϕ is a complex function of x and y. The first two terms in the above equation correspond to the optical potential that supports constant-intensity (CI) waves [1–3]. We also note that this form of the optical potential is related to the class of Bohmian non-Hermitian potentials derived in [4], which are two-dimensional generalizations of the Wadati potentials for arbitrary waveforms. The important feature to emphasize, however, is that in our case $\phi(x,y)$ is itself a solution of the Helmholtz equation.

B. Non-Hermitian mapping for Gaussian and flattened Gaussian beams

We examine the propagation of beams of finite width through disordered media. In particular, such media can be described by an arbitrary smooth and real function $\theta(x,y)$. Throughout the main text and the supplementary material (apart from Fig. 1 of the main text, where the case of a simple dipole potential is presented) we consider $\theta(x,y)$ to be a superposition of $N = 300$

Gaussians with random-valued amplitudes V_n and widths σ_n, randomly distributed around center positions x_n, y_n,

$$\theta(x,y) = \sum_{n=1}^{N} V_n e^{-(\frac{x-x_n}{\sigma_n})^2-(\frac{y-y_n}{\sigma_n})^2}. \tag{S9}$$

In addition, we also need to determine the reference solution $\phi(x,y)$ in homogeneous space, which we choose to be a Gaussian beam. Since there are no compact analytical beam solutions of the Helmholtz equation even in homogeneous space, our first approach is to rely on the paraxial solutions of the wave equation. Specifically, we expect this approximation to work well for beams with transverse widths several times the wavelength λ. In particular, we examine the propagation of Gaussian, flattened Gaussian beams [5] and plane waves (approximated by super-Gaussians), for which cases the following analytical solutions are available in the regime of paraxial approximation [6, 7]:

$$\phi_G(x,y) = \frac{e^{\frac{-y^2}{w_0^2}+i\left(n_{ref}kx-\arctan(\frac{x}{x_R})+\frac{n_{ref}ky^2}{2\left(x+\frac{x_R^2}{x}\right)}\right)}}{\sqrt{1+\frac{x^2}{x_R^2}}}, \tag{S10}$$

for a Gaussian beam, and the solution:

$$\phi_F(x,y) = \sum_{m=1}^{M} \kappa_m \frac{e^{\frac{-my^2}{w_0^2}+i\left(n_{ref}kx-\arctan(\frac{mx}{x_R})+\frac{n_{ref}ky^2}{2\left(x+\frac{x_R^2}{m^2x}\right)}\right)}}{\sqrt{1+\frac{m^2x^2}{x_R^2}}}, \tag{S11}$$

for a flattened Gaussian beam (which is a sum of M Gaussians) propagating in the x-direction, where

$$\kappa_m = \frac{(-1)^{m-1}}{M}\binom{M}{m}, \tag{S12}$$

w_0 is the Gaussian width and $x_R = \pi w_0^2 n_{ref}/\lambda$. For beams propagating along a direction that forms an angle α with the x-axis of the rectangular scattering region defined by $[-L_x, L_x]$ and $[-L_y, L_y]$, a simple coordinate transformation is used: $x \to x\cos\alpha + y\sin\alpha$, $y \to -x\sin\alpha + y\cos\alpha$, to rotate the propagation axis of the above solutions.

2. GAUSSIAN BEAM PROPAGATION

Having these closed form solutions that describe finite paraxial beams and an expression for the random medium, we can directly calculate the corresponding complex refractive index distribution. More specifically, we now apply the relation Eq. (S8) to construct optical potentials that relate the propagation of a Gaussian beam in homogeneous space to the diffraction of a Gaussian beam in a non-Hermitian medium. By substituting the paraxial solution $\phi_G(x,y)$ given by Eq. (S10), and the function $\theta(x,y)$ given by Eq. (S9) into the relation Eq. (S8), we obtain the dielectric function $\varepsilon(x,y)$ of the problem.

A. Parametric study of sensitivity

In the main text we have examined the propagation of a Gaussian beam through a disordered potential generated by a $\theta(x,y)$ given by Eq. (S9) for $N = 300$. The corresponding real and imaginary parts of the refractive index, given by $n(x,y) = \sqrt{n_{ref}^2 + \varepsilon(x,y)}$, along with the electric field intensities, are depicted in Fig. 2 of the main text.

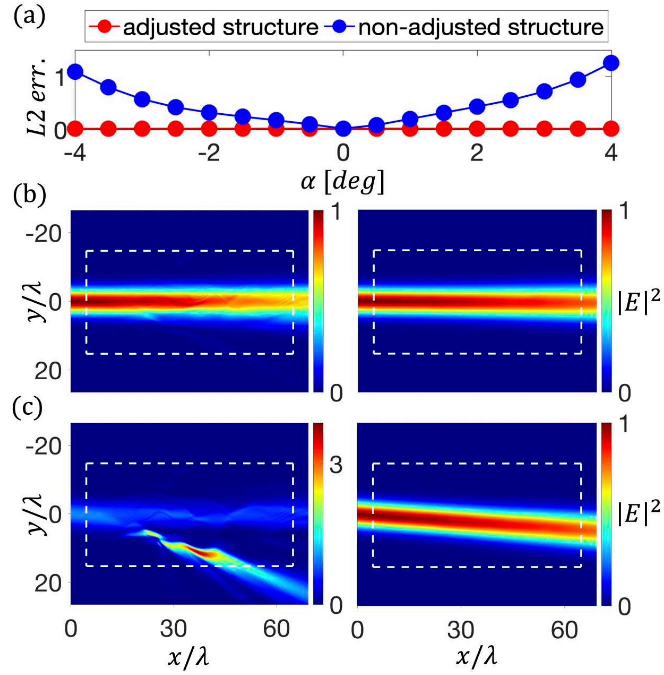

Fig. S1. Sensitivity of the distribution Eq. (S8) for a Gaussian beam of width $w_0 = 5\lambda$, to changes in the incidence angle α. (a) The relative L2 error [see Eq. (S13)] inside the scattering region [defined by the white dashed lines in (b) and (c)] increases for increasing $|\alpha|$ if the refractive index distribution designed for $\alpha = 0°$ is used (blue dots, lines are guide to the eye). When adapting the design of the dielectric function to each input angle $\alpha \neq 0°$, the corresponding L2 error stays near zero (red dots, lines are guide to the eye). (b) The intensity of the scattered beam for an incidence angle of $\alpha = 0.5°$. In the two sub-figures (left vs. right) the electric field intensity is shown for a beam propagating in the refractive index distribution designed for incidence at $\alpha = 0°$ (left) and $\alpha = 0.5°$ (right), respectively. (c) Same as in (b) but for a beam impinging at $\alpha = 4°$ on a potential with a design for $\alpha = 0°$ (left) and $\alpha = 4°$ (right).

Here we wish to explore the sensitivity of our approach to changes in the incidence angle and frequency detuning of the beam as it propagates through the scattering medium. To quantify the degree of deviation from the numerically calculated free space solution we use the relative L2 error, defined as

$$d(I, I^f) = \frac{\sqrt{\int_{-L_x}^{L_x}\int_{-L_y}^{L_y}[I(x,y) - I^f(x,y)]^2 dxdy}}{\sqrt{\int_{-L_x}^{L_x}\int_{-L_y}^{L_y}[I^f(x,y)]^2 dxdy}}, \tag{S13}$$

where $I(x,y)$ is the intensity distribution of a propagating beam in a non-Hermitian landscape $\varepsilon(x,y)$ with given input parameters, and $I^f(x,y)$ is the intensity distribution for the same input beam parameters, but in a homogeneous medium with a dielectric constant n_{ref}^2.

In Fig. S1a we show the dependence of the scattered fields on the incidence angle α for the cases of a Gaussian beam $\phi_G(x,y)$ propagating in a complex potential that is designed according to the relations of Section 1 to guide a Gaussian beam at $\alpha = 0°$ or at the adjusted angle $\alpha \neq 0°$. Our results demonstrate

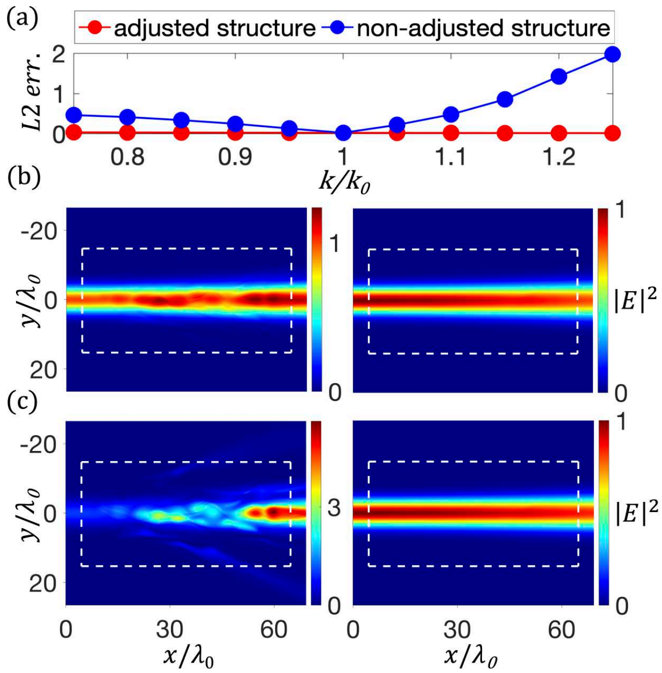

Fig. S2. Sensitivity of the Gaussian beam propagation through a dielectric distribution Eq. (S8) to wavenumber k-detuning. (a) The relative L2 error [Eq. (S13)] inside the scattering region [defined by the white dashed lines in (b) and (c)] increases the higher the detuning of k is from the design value k_0 (blue dots, lines are guide to the eye). The error stays near zero when the design value is adjusted to the angle of the beam input (red dots, lines are guide to the eye). (b) The intensity of the scattered beam with $k = 1.05k_0$. In the two sub-figures (left vs. right) the electric field intensity is shown for a beam propagating in the dielectric distribution corresponding to a design wavenumber k_0 (left) and $1.05k_0$ (right), respectively. (c) Same as in (b) but for $k = 1.25k_0$. In all cases shown the width of the Gaussian beam is $w_0 = 5\lambda_0$.

that the degree of deviation of a beam's intensity from the free-space case increases for an increasing mismatch between the potential design angle and the actual angle of an incoming beam. When the design of the potential is adjusted to the angle of the incoming beam the deviation always stays below 0.024. The reason for a nonzero L2 value for a potential adjusted to the correct incidence angle is due to the fact that Eq. (S10) is only an approximate solution of the homogeneous Helmholtz problem, and the width of the beam is $w_0 = 5\lambda$. In Figs. S1b,c several characteristic examples of the intensity profiles of such beams are provided.

In Fig. S2 we show the dependence of the scattered fields on the beam's wavenumber k for the cases of a Gaussian beam $\phi_G(x, y)$ entering a medium described by $\varepsilon(x, y)$ according to the relations of Section 1 for the two cases: (i) $k = k_0$ and (ii) $k \neq k_0$. When we consider the dielectric distribution of Eq. (S8) designed for a k_0 wavenumber, the system again shows a sensitivity to the input k value, whereas the design adjusted to $k \neq k_0$ always stays below 0.04 error (see the discussion above). For the former case the beam's intensity modulations start getting increasingly larger for beams with wavenumbers k that are detuned more than 5% from the k_0 value, which is relatively wide, e.g., for laser beams near the visible range of the spectrum.

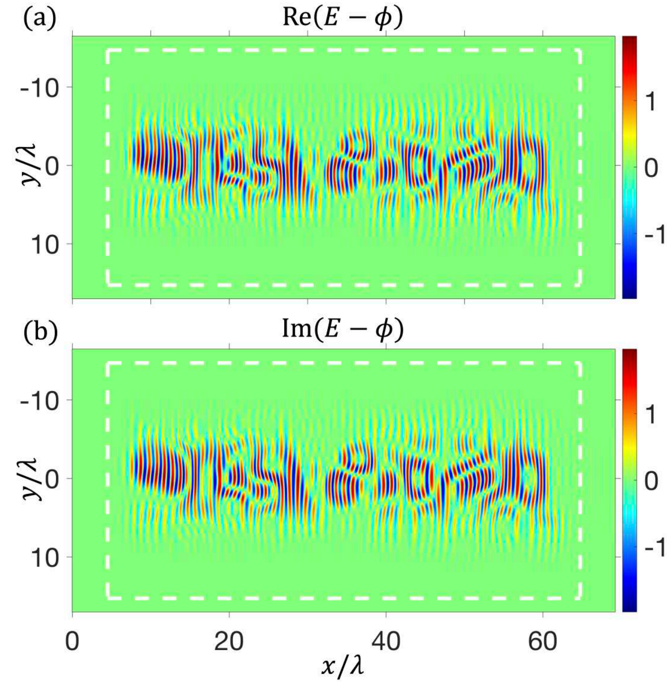

Fig. S3. Comparison of the non-Hermitian potential solution $E(x, y)$ to the homogeneous space solution $\phi(x, y)$ for the case presented in Fig. 2 of the main text. We present the difference between (a) the real and (b) the imaginary part of these two solutions, respectively. We can see that the two solutions have both equal amplitude and phase outside of the scattering region (dashed lines), but not inside (the beam's width here is smaller than the scattering region).

The robustness of the pre-designed dielectric function Eq. (S8) to variations of the incidence angle α and of the wavenumber k, depends on both the shape, amplitude and length scale of the $\varepsilon(x, y)$ distribution produced by $\theta(x, y)$, as well as, on the form of the free space solution $\phi(x, y)$. Due to the complex multiple scattering occurring in a highly disordered medium, such as the one shown in Fig. 2a of the main text, it is expected that our designed refractive index distributions are indeed sensitive to changes of the incidence angle or the wavenumber. Still, however, the demonstrated degree of sensitivity is much lower than for the case that our mapping procedure was based on a resonance effect inside the medium (for similar considerations in a one-dimensional CI-problem see [8]).

B. Unidirectional invisibility

In this paragraph we discuss the unidirectional invisibility of the refractive index distribution shown in Figs. 2a,b of the main text. A potential can be considered unidirectionally invisible if neither measurements of phase nor amplitude outside the scattering region can detect the presence of an inhomogeneous refractive index distribution. As noted in the main text, the design principle of Eq. (S8) automatically generates unidirectionally invisible potentials for functions $\theta(x, y)$ that vanish outside of the scattering region (as assumed here). The potentials used throughout this paper are thus indeed unidirectionally invisible for the beam and the wavenumber they are designed for.

To demonstrate this explicitly, we plot the difference between the electric fields E and ϕ throughout the simulated space. In

Figs. S3a,b we show that both the real and the imaginary part of this difference vanish outside of the scattering region, but not inside. This, along with the intensity plot of Fig. 2 in the main text, indeed confirms that the solutions in a potential generated by the refractive index distribution of Eq. (S8) with $\theta(x, y)$ given by Eq. (S9) exhibit the amplitude and phase distribution of homogeneous space everywhere outside of the scattering region (but not inside, where only the intensities are equal).

An important additional feature is the broadband character of the potentials' unidirectional invisibility, which we now investigate by comparing the behavior of the non-Hermitian potential at the design value of $k = k_0$ with the corresponding behavior in homogeneous space. In particular, we examine how the electric field profiles at the end of the scattering region change when we detune the wavenumber k away from the design value k_0 (of course without readjusting the non-Hermitian potential in this detuning process). The results that show the deviations of the real and imaginary parts of the non-Hermitian solution from the homogeneous space reference solution at $k = k_0$ are shown in Fig. S4. The plots demonstrate that the wavenumber detuning has a very similar effect on the output profiles of the beam when propagating through the non-adjusted non-Hermitian potential and through homogeneous space, respectively. In fact, the complex electric field profiles at the end of the medium are nearly equal to the free space profiles for a relatively broad region of $\pm 5\%$ around the design frequency $k = k_0$. Our refractive index distribution thus allows us to generate a new class of potentials that are unidirectionally invisible in a broadband frequency interval, even for highly disordered scattering environments. This intriguing feature offers the exciting prospect of scattering-free pulse propagation through such invisible non-Hermitian media, as studied earlier in 1D scattering potentials [8].

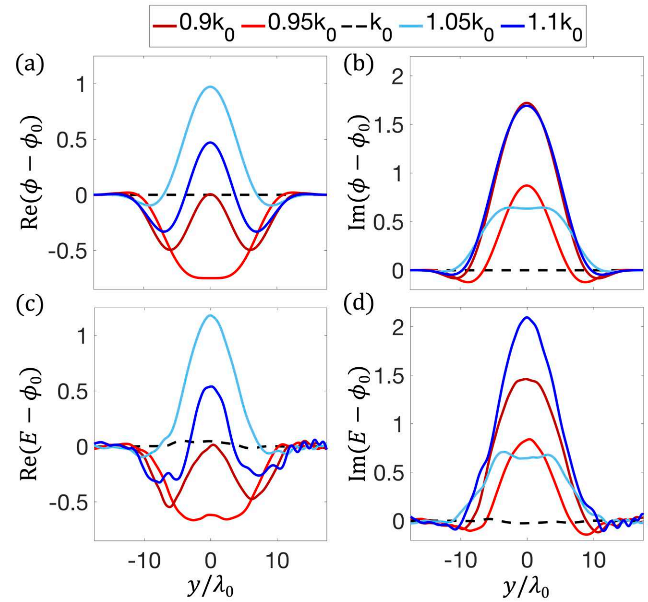

Fig. S4. Effect of wavenumber detuning on the output field profile of the Gaussian beam propagating through homogeneous space (ϕ, top row) and through the non-Hermitian disordered system considered in Fig. 2 of the main text (E, bottom row). In all panels we plot the deviations of the output field profiles $\phi(x = L_x, y)$ and $E(x = L_x, y)$ from the reference solution $\phi_0(x = L_x, y)$ in homogeneous space at the design frequency of $k = k_0$. These deviations are recorded directly at the distal end of the scattering region (at $x = L_x$), in both their real (left column) and imaginary parts (right column), for different input k-values (see different line colors). The similarity between the deviations in the homogeneous space (top row) and the non-adujsted non-Hermitian potential (bottom row) demonstrates the broadband character of the uni-directional invisibility for potentials following our design. The k-values plotted are: $k = 0.9k_0$ (dark red, solid), $k = 0.95k_0$ (light red, solid), $k = k_0$ (black, dashed), $k = 1.05k_0$ (light blue, solid) and $k = 1.1k_0$ (dark blue, solid). The deviations in the non-Hermitian profiles resemble those in homogeneous space for k-values inside a range of $\pm 5\%$ around the design frequency k_0. The displayed data were taken from cross sections of the fields of Fig. S2, where all solutions are calculated numerically. The small deviations from the ϕ_0 field observed in (c) and (d) for the $k = k_0$ non-Hermitian case (dashed black lines) can be attributed to the paraxial approximation. More specifically, the solution that was inserted into the relation for the non-Hermitian potential (S8) (see Section 1B) is exact only in the paraxial limit.

3. RELATION TO THE TWO-DIMENSIONAL CI-WAVES

A. Plane waves and CI-waves

In this section we will examine the relation of the above results to the two-dimensional CI-waves. Let us consider for this purpose a plane wave solution of Eq. (S2). If we assume an arbitrary propagation direction in the $x - y$ plane, we have the solution:

$$\phi(x, y) = e^{in_{ref}k_x x + in_{ref}k_y y}, \tag{S14}$$

with the corresponding dispersion relation:

$$k_x = \pm\sqrt{k^2 n_{ref}^2 - k_y^2}, \tag{S15}$$

for forward or backward propagating plane waves in the homogeneous bulk space. By substitution into Eq. (S8), we get:

$$\varepsilon(x, y) = (\nabla\theta)^2 - \frac{i}{k}\left(\nabla^2\theta + 2in_{ref}\mathbf{k}\cdot\nabla\theta\right). \tag{S16}$$

It is useful to note that the extra term is related to the power flow of the Poynting vector (see below). If the plane wave is propagating only parallel to the x-axis then $k_y = 0$ and therefore we have:

$$\varepsilon(x, y) = (\nabla\theta)^2 - \frac{i}{k}\nabla^2\theta + 2n_{ref}\frac{\partial\theta}{\partial x}. \tag{S17}$$

The corresponding two-dimensional CI-wave solution is then:

$$E_{CI}(x, y) = e^{in_{ref}kx}e^{ik\theta(x,y)} = e^{ik\theta_{CI}(x,y)}, \tag{S18}$$

where $\theta_{CI}(x, y) = n_{ref}x + \theta(x, y)$. It is easy to show that the corresponding potential $\varepsilon_{CI}(x, y) = n_{ref}^2 + \varepsilon(x, y)$ producing this solution is given by: $\varepsilon_{CI}(x, y) = (\nabla\theta_{CI})^2 - \frac{i}{k}\nabla^2\theta_{CI}$, which is the potential that supports two-dimensional CI-waves, namely a generalization of the Wadati potential in two dimensions [1].

B. Boundary conditions

In this paragraph we examine how the extra term of the solution Eq. (S17) is related to the boundary conditions of the CI-wave problem. Without loss of generality, we assume that a plane wave of the form e^{ikx} is incident onto the medium. Then we

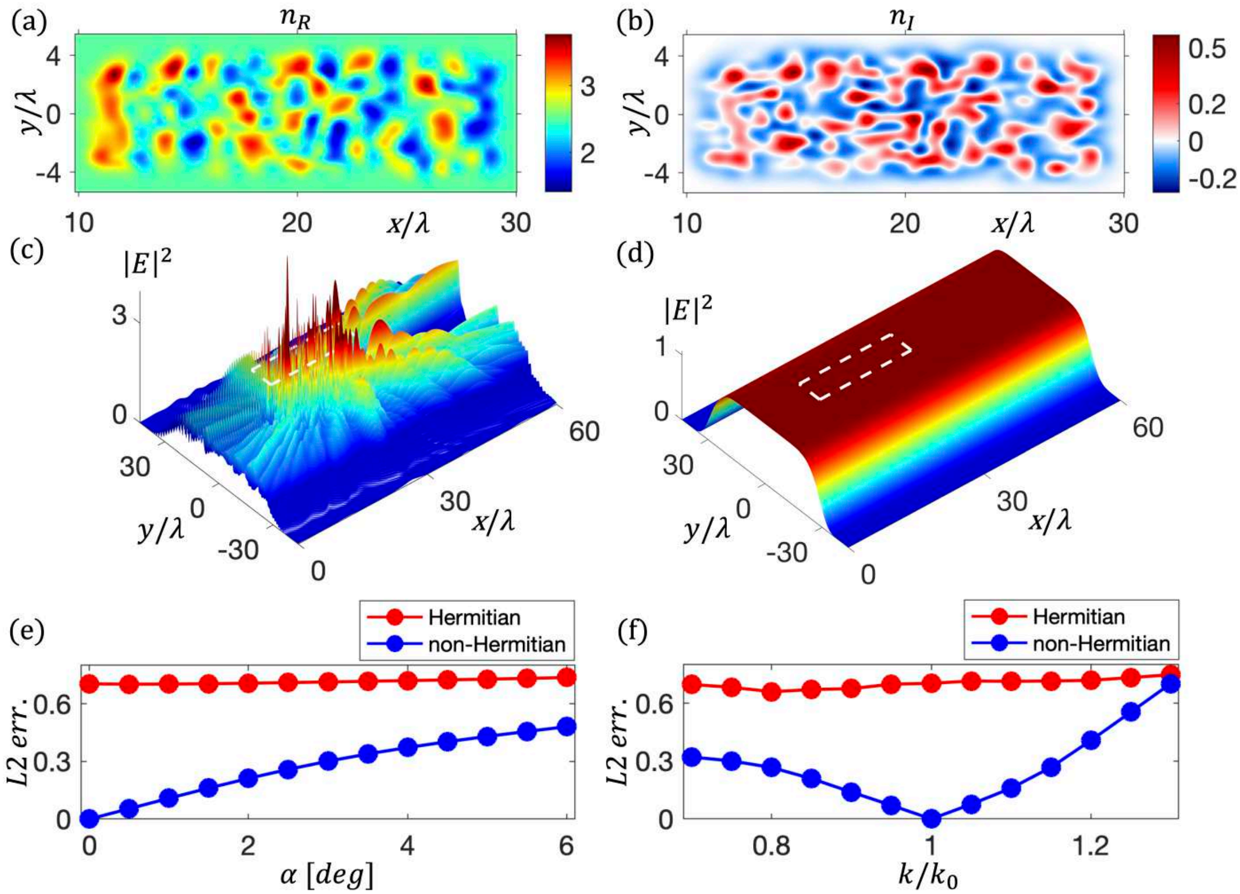

Fig. S5. Complex scattering of a super-Gaussian beam that is wider than the scattering region of a disordered medium. We study the sensitivity of the $\varepsilon_{CI}(x,y)$ optical potential (see text) that eliminates multiple scattering and interference effects. The components of the non-Hermitian refractive index distribution $n(x,y)$ are plotted in (a), (b) for the real and imaginary parts, respectively. Propagation inside (c) a Hermitian $[n(x,y) = n_R(x,y)]$ and (d) a non-Hermitian $[n(x,y) = n_R(x,y) + in_I(x,y)]$ medium reveals that the CI-wave distribution works well to mitigate the multiple scattering and interference effects for a super-Gaussian beam of a large width. The white dashed rectangles in (c) and (d) denote the limits of the scattering region, depicted in (a) and (b). Relative L2 errors (see relation Eq. (S13)) inside the region marked by a rectangle were calculated for the Hermitian (red dots, lines are guide to the eye) and non-Hermitian (blue dots, lines are guide to the eye) cases, for varying (e) the beam's incidence angle α and (f) the value of the k-vector of the beam.

are lead to impose the perfect transmission boundary conditions along the x-axis (at the endpoints of the scattering region $x = \pm L_x$, for every value of y) and continuity conditions along the y-axis. In other words, we have the following six boundary conditions for the electric field E_{CI} and its derivative (corresponding to the magnetic field):

$$\frac{\partial E_{CI}}{\partial x}(\pm L_x, y) = ikE_{CI}(\pm L_x, y)\,, \tag{S19}$$

$$E_{CI}(x, \pm L_y)^+ = E_{CI}(x, \pm L_y)^-\,, \tag{S20}$$

$$\frac{\partial E_{CI}}{\partial y}(x, \pm L_y)^+ = \frac{\partial E_{CI}}{\partial y}(x, \pm L_y)^-\,. \tag{S21}$$

By direct substitution of the CI-wave solution Eq. (S18), we can rewrite the above boundary conditions in terms of $\theta_{CI}(x,y)$ as: $\frac{\partial \theta_{CI}}{\partial x}(\pm L_x, y) = n_{ref}$, $\theta_{CI}(x, \pm L_y) = n_{ref}x$, $\frac{\partial \theta_{CI}}{\partial y}(x, \pm L_y) = 0$. Choosing now a $\theta(x,y)$ function that obtains zero values at the boundaries of the scattering region, we can write $\theta_{CI}(x,y) = n_{ref}x + \theta(x,y)$. The dielectric function $\varepsilon_{CI}(x,y)$ can then be expressed as

$$\varepsilon_{CI}(x,y) = n_{ref}^2 + (\nabla\theta)^2 - \frac{i}{k}\nabla^2\theta + 2n_{ref}\frac{\partial\theta}{\partial x}\,, \tag{S22}$$

which is exactly the form of Eq. (S17), offset by n_{ref}^2. The extra term in the relation Eq. (S17), derived by our mapping approach, thus ensures that the CI-wave solution preserves the global power flow in the direction of the initial plane wave, which are indeed the perfect transmission boundary conditions (see next paragraph).

C. Poynting vector

The physical meaning of the boundary conditions at $x = \pm L_x$ can be explained in terms of power flow. In particular, the power flow is described by the Poynting vector of a linearly polarized electric field $E_{CI}(x,y) = e^{i\theta_{CI}(x,y)}$:

$$\mathbf{S} = \frac{i}{2}(E_{CI}\nabla E_{CI}^* - E_{CI}^*\nabla E_{CI}) = k\nabla\theta_{CI} = kn_{ref}\hat{\mathbf{x}} + k\nabla\theta. \tag{S23}$$

The perfect transmission boundary condition of Eq. (S19) thus ensures the power flow will have only a $+x$-component at the $x = \pm L_x$ boundaries (where $\nabla\theta = 0$). The boundary conditions also give rise to the $\frac{\partial\theta}{\partial x}$ term of Eq. (S22). This term is related to the $\nabla\theta$ term of the above expression, giving global flow only in the $+x$-direction. In other words, the existence of CI-waves is directly related to the perfect transmission boundary conditions, which are in turn related to the power flow engineering by using suitable distributions of gain and loss.

D. Parametric study of sensitivity

Inspired by the CI-wave solution, we now consider the case of a super-Gaussian beam with a width larger than the scattering region, propagating in a disordered complex potential with real and imaginary parts depicted in Fig. S5a,b, respectively. We choose a $\theta(x, y)$ function that is determined by Eq. (S9) with $N = 300$, and satisfies the boundary conditions of Eqs. (S19-S21).

Neglecting the beam broadening (since the beam is much wider than the scattering region and the wavelength), we can approximate the electric field of the homogeneous problem by $\phi(x, y) \approx e^{in_{ref}kx}e^{-y^8/\xi^8}$. This gives for the third term of the expression (S8): $2n_{ref}\frac{\partial\theta}{\partial x} + \frac{2i}{k}\frac{y^7}{\xi^8}\frac{\partial\theta}{\partial y}$. The first term of this expression is a consequence of power flow in the $+x$-direction, whereas the second term is neglected in our case since $\xi = 32.03\lambda$ and the scattering region in the y-direction is approximately located in the interval $[-5\lambda, 5\lambda]$. The results of Fig. S5d demonstrate that including the appropriate term in the non-Hermitian potential using expression Eq. (S8), leads to a perfect constant intensity wave that propagates both inside and outside of a medium and cancels reflection and multiple scattering effects that are present in the corresponding Hermitian potential as shown in Fig. S5c. To test the sensitivity of the designed disordered non-Hermitian optical potential we vary the incidence angle α and the k-vector of the beam (at normal incidence) and plot the relative L2 error defined by Eq. (S13). Near normal incidence, the CI-wave distribution works well and produces a beam without intensity modulations, as compared to the Hermitian case. At angles larger than 5° the non-Hermitian and Hermitian solutions start having similar error with comparison to the intensity distribution in homogeneous space, marking the limits of validity of our non-Hermitian design Eq. (S8), which produces constant-intensity waves. The k-vector scan shows a relatively higher degree of robustness. The design starts to fail for deviations of around 10% from the design wavenumber. Our results are presented in Fig. S5e, and Fig. S5f for the sensitivity on variations of the angle of incidence and the wavenumber, respectively.

E. Limits of validity of the CI-wave permittivity distribution

As demonstrated above, the additional term stemming from the spatially varying beam profile can be neglected for our super-Gaussian since it has a width larger than the scattering region. This is not the case for beams with transverse widths comparable to the width of the scattering region. To test this explicitly, we investigate in this paragraph the propagation of a flat top Gaussian beam through disordered non-Hermitian media described by Eq. (S8). We choose a flattened Gaussian solution $\phi_F(x, y)$ defined by Eq. (S11) for $M = 4$. Since there is no convenient closed form expression of the homogeneous non-paraxial Helmholtz equation for a finite beam, we rely on the paraxial solution [6, 7], which is valid for transverse widths down to approximately a few wavelengths λ.

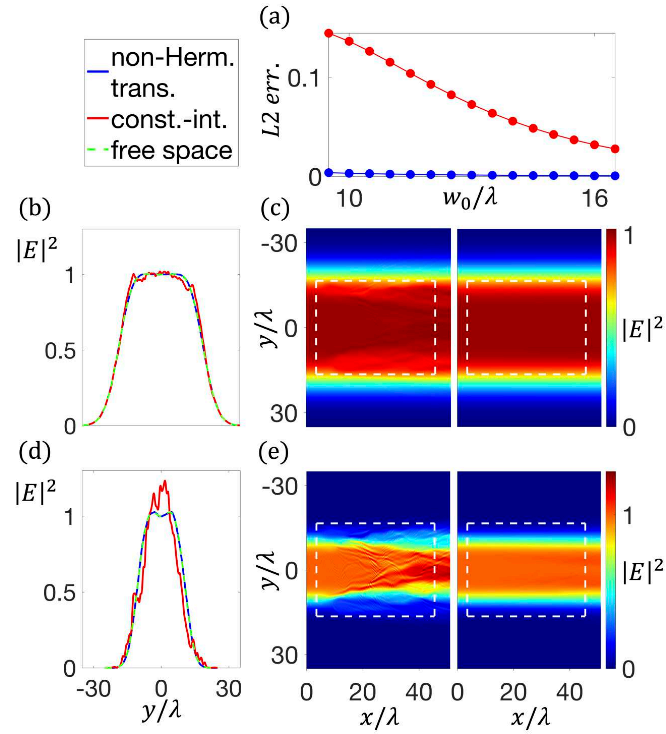

Fig. S6. Validity limits of the CI-wave refractive index distribution for flattened Gaussian beams with $M = 4$ [see Eq. (S11)] and widths smaller than the scattering region. (a) The relative L2 error [Eq. (S13)] inside the scattering region [white dashed lines in (c) and (e)] increases for reducing w_0 if the CI-wave distribution is used (red dots, lines are guide to the eye), whereas it stays near zero if the mapping Eq. (S8) is used. The refractive indices of the respective problems are shown in Figs. 2a,b and Fig. 4a of the main text. (b) Beam's profile at the end of the plotted area for $w_0 = 16.5\lambda$ (red solid line: CI-wave distribution, blue solid line: non-Hermitian mapping, green dashed line: solution of the homogeneous medium). (c) Intensity distributions for the same width in the case of CI-wave (left) and non-Hermitian mapping (right) potentials. Plots in (d), (e) are equivalent to (b), (c) but for $w_0 = 9.5\lambda$.

We now compare the CI ansatz to the full non-Hermitian potential with the extra term (which is important when beam broadening cannot be ignored). The plots of relative L2 error for the two cases against the flattened Gaussian width w_0 are shown in Fig. S6. For large values of w_0, the two distributions produce similar solutions (see figure panels b,c), where the flat part of the beam passes through the medium with little or no distortion. When the beam's width is reduced to values comparable to the transverse scattering region dimensions ($\approx 10\lambda$), then the CI solution starts to deviate from the one in homogeneous space, and scattering and interference effects cause significant distortion to the beam profile both inside and outside of the medium (see Fig. S6d,e). When the non-Hermitian potential's width is adjusted to the incoming beam we observe a nearly perfectly undistorted propagation down to lower than $w_0 \approx 10\lambda$ (meaning the smallest Gaussian in expansion (S11) is less than 5λ wide), which is also close to the limit of validity of the paraxial approximation [6, 7].

REFERENCES

1. K. G. Makris, Z. H. Musslimani, D. N. Christodoulides, and S. Rotter, *Constant-intensity waves and their modulation instability in non-Hermitian potentials*, Nat. Commun. **6**, 7257 (2015).
2. K. G. Makris, A. Brandstötter, P. Ambichl, Z. H. Musslimani, and S. Rotter, *Wave propagation through disordered media without backscattering and intensity variations*, Light Sci. Appl. **6**, e17035 (2017).
3. E. Rivet, A. Brandstötter, K. G. Makris, H. Lissek, S. Rotter, and R. Fleury, *Constant-pressure sound waves in non-Hermitian disordered media*, Nat. Phys. **14**, 942 (2018).
4. S. Yu, X. Piao, and N. Park, *Bohmian photonics for independent control of the phase and amplitude of waves*, Phys. Rev. Lett. **120**, 193902 (2018).
5. F. Gori, *Flattened gaussian beams*, Opt. Commun. **107**, 335 (1994).
6. A. Yariv, and P. Yeh, *Optical Waves in Crystals*, Wiley Interscience, 1st Edition (1983).
7. A. Yariv, *Photonics: Optical Electronics in Modern Communications*, Oxford University Press (2006).
8. A. Brandstötter, K.G. Makris, and S. Rotter, *Scattering-free pulse propagation through invisible non-Hermitian media*, Phys. Rev. B **99**, 115402 (2019).